This document is downloaded from DR-NTU (https://dr.ntu.edu.sg)
Nanyang Technological University, Singapore.

Plasmon-enhanced hydrogen evolution on Au-InVO4 hybrid microspheres

Cao, Shao-Wen; Fang, Jun; Mohammad Mehdi Shahjamali; Boey, Freddy Yin Chiang; Barber, James; Loo, Say Chye Joachim; Xue, Can

2012

Cao, S. W., Fang, J., Mohammad, M. S., Boey, F. Y. C., Barber, J., Loo, S. C. J., et al. (2012). Plasmon-enhanced hydrogen evolution on Au-InVO4 hybrid microspheres. RSC advances, 2(13), 5513-5515.

https://hdl.handle.net/10356/94635

https://doi.org/10.1039/C2RA20405C

© 2012 Royal Society of Chemistry. This is the author created version of a work that has been peer reviewed and accepted for publication by RSC Advances, Royal Society of Chemistry. It incorporates referee’s comments but changes resulting from the publishing process, such as copyediting, structural formatting, may not be reflected in this document. The published version is available at: [DOI: http://dx.doi.org/10.1039/C2RA20405C]

Downloaded on 09 Feb 2023 20:30:49 SGT

Plasmon-Enhanced Hydrogen Evolution on Au-$InVO_4$ Hybrid Microspheres

Shao-Wen Cao,[a] Jun Fang,[a] Mohammad Mehdi Shahjamali,[a] Freddy Y. C. Boey,[a] James Barber,[a, b] Say Chye Joachim Loo*[a] and Can Xue*[a]

Received (in XXX, XXX) Xth XXXXXXXXX 20XX, Accepted Xth XXXXXXXXX 20XX
DOI: 10.1039/b000000x

We demonstrate the plasmon-enhanced hydrogen evolution from photocatalytic water reduction by using Au-$InVO_4$ hybrid microspheres. The surface plasmons of gold nanoparticles enhance the sub-band gap excitation of InVO4 and promote charge separation on its surfaces through plasmon-exciton coupling, thereby significantly improve their photocatalytic efficiency.

Solar-to-fuels conversion through photocatalytic water splitting has been recognized as highly important energy sources for the sustainable future.[1] Researchers have made tremendous efforts to develop various visible-light-active metal oxide photocatalysts, such as $BiVO_4$,[2,3] Fe_2O_3,[4,5] and Cu_2O,[6,7] for water oxidation or reduction. Ye and co-workers have reported a new type of metal oxide $InVO_4$ which is capable of producing H_2 through visible-light driven photocatalytic water reduction.[8,9] Recent studies revealed that the actual band-to-band energy gap of $InVO_4$ could be more than 3 eV, while its visible-light activities were attributed to sub-band gap transitions from impurity states.[10-12] Though it is certainly beneficial from extended absorption in the visible range, the impurity states will also promote undesirable recombination of photogenerated electrons and holes, which may reduce the photocatalytic activities. Consistently, some researchers also found that their prepared $InVO_4$ structures are unviable to show visible-light-driven hydrogen production due to inefficient charge separation from visible-light-induced sub-band gap transition.[12-14]

In order to achieve high photocatalytic activities, efficient charge separation is crucial for all photocatalysts. To date, researchers have developed many different methods to enhance the separation of photogenerated electrons and holes. One promising approach is depositing plasmonic particles of noble metals (e.g. Au and Ag) onto the photocatalysts.[15-17] As well known, gold and silver nanoparticles exhibit strong surface plasmon resonance (SPR) in the visible range.[18,19] It has been demonstrated that the SPR of metal nanoparticles would greatly promote the photocatalytic efficiencies of metal oxide photocatalysts because the SPR-enhanced localized electric field can improve the charge separation near the metal-semiconductor interfaces.[20,21]

Herein, we report a new strategy to utilize gold SPR to enhance visible-light-driven hydrogen evolution through photocatalytic water reduction by using Au-$InVO_4$ hybrid microspheres prepared by growing gold nanoparticles on pre-synthesized $InVO_4$ hollow microspheres. We demonstrate that the gold nanoparticle SPR can significantly enhance the sub-band gap transition of $InVO_4$ microspheres and thereby their photocatalytic efficiencies. The detailed plasmonic effect on charge separation is also discussed in-depth.

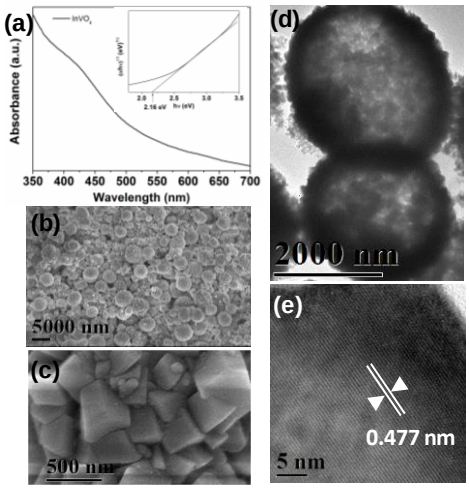

Fig. 1 (a) UV-vis spectrum of $InVO_4$ microspheres, inset is the plot of $(\alpha h\nu)^{1/2}$ *vs* photon energy ($h\nu$) to calculate the band gap; (b, c) SEM images and (d, e) TEM images of $InVO_4$ microspheres.

The prepared $InVO_4$ sample is identified as orthorhombic phase through XRD analyses (Fig. S1). The absorption spectrum (Fig. 1a) shows that the $InVO_4$ sample exhibits obvious absorption in the visible light range with a band gap estimated as 2.16 eV. The analyses by SEM and TEM (Fig. 1b-d) reveal that the sample consists of hollow microspheres that are built by assembly of many $InVO_4$ nanocrystals. The high-resolution TEM image (Fig. 1e) of the nanocrystal indicates a fringe spacing of 0.477 nm in accordance with the lattice spacing of the (110) plane of orthorhombic $InVO_4$.

Three Au-$InVO_4$ hybrid samples with different Au content were prepared by reducing $HAuCl_4$ with L-ascorbic acid in the presence of $InVO_4$ microspheres and L-cysteine that can bind to the $InVO_4$ surface through its carboxylate group and captured gold onto $InVO_4$ surfaces via the Au–S bonding.[22,23] SEM and TEM images (Fig. 2a, S2, S3, S4) indicate that gold nanoparticles were successfully grown onto the $InVO_4$ microspheres and the original microsphere morphology did not change during the gold nanoparticle growth process. The gold contents in these three samples were estimated as ~2 wt%, 4 wt%, and 7.5 wt%, respectively, according to the analyses by energy-dispersive X-ray (EDX) spectroscopy. The high-magnification TEM images (Fig. S2-S4) reveal that the sizes of gold nanoparticles in these samples are 3.7 (±0.9) nm, 6.7 (±1.5) nm, and 13.0 (±1.9) nm, respectively. The SPR feature of gold nanoparticles can be clearly observed at ~540 nm for the 4 wt% and 7.5% wt% Au-$InVO_4$ samples (Fig. 2b). The absence of SPR feature for the 2 wt% Au-$InVO_4$ sample may be due to the low concentration of gold nanoparticles. In addition, the SPR of small gold particles (<5 nm) is usually very weak,[24] and may be overwhelmed by $InVO_4$ absorption.

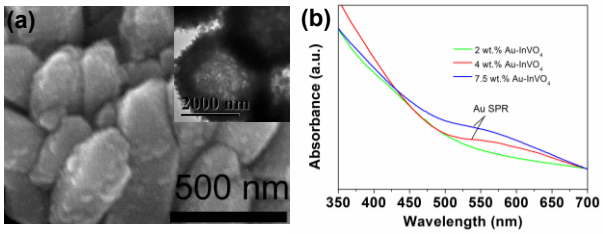

Fig. 2 (a) SEM and TEM image (inset) of 4 wt% Au-$InVO_4$ microspheres; (b) UV-vis spectra of 2, 4, 7.5 wt% Au-$InVO_4$ samples.

The prepared Au-$InVO_4$ hybrid microspheres were then tested for photocatalytic H_2 evolution under visible-light (λ > 420 nm) irradiation. L-ascorbic acid (0.1 M, pH=4.0) was used as the electron donor. Fig. 3a shows the H_2 evolution plots by different samples as a function of irradiation time. In comparison to pure $InVO_4$ microspheres that showed no H_2 evolution, all Au-$InVO_4$ hybrid microspheres exhibit obvious visible-light-driven photocatalytic activity for H_2 evolution. Among them, the 4 wt% Au-$InVO_4$ sample showed the highest H_2 evolution rate of 116.7 $\mu mol \cdot h^{-1} \cdot g^{-1}$ which then dropped to 15.9 $\mu mol \cdot h^{-1} \cdot g^{-1}$ after 90 min and became quite stable thereafter (Fig. S5). The stable H_2 evolution rate (after 90 min) of the 2 wt% and 7.5 wt% Au-$InVO_4$ samples were 12.5 $\mu mol \cdot h^{-1} \cdot g^{-1}$ and 8.6 $\mu mol \cdot h^{-1} \cdot g^{-1}$, respectively.

As well known, semiconductor photocatalysts can have improved efficiencies after loaded with nanoparticles of noble metals such as Pt, Pd and Au.[25,26] The metal nanoparticles can act as electron sinks to hold the excited electrons from the semiconductor band-gap excitation, which retard the charge recombination process and thereby increases its photocatalytic efficiency.[27] In order to clarify whether the electron-sink effect dominates in the Au-$InVO_4$ samples, we prepared Pt-$InVO_4$ hybrid microspheres with 4 wt% Pt by using similar methods (Fig. S6). The XPS analyses (Fig. S7) reveal the binding energy of Au 4f (84.1 and 87.8 eV) and Pt 4f (71.2 and 74.6 eV), indicating the zero-valent nature of the deposited gold and platinum. However, after visible-light irradiation for 3 hours, the photocatalytic H_2 evolution amount of this Pt-$InVO_4$ sample (5.0 umol/g) is much lower than that of the 4 wt% Au-$InVO_4$ sample (167.1 umol/g) (Fig. 3b). The Pt-$InVO_4$ samples with less Pt loading (1 wt% and 2 wt%) showed even smaller H_2 evolution amount (Fig. S8). This comparison result suggests that the pure electron-sink effect only play a minor role for the metal-$InVO_4$ hybrids as it's well known that Pt is usually more active than Au for H_2 evolution due to the lower H_2 evolution overpotential on Pt surfaces.[28]

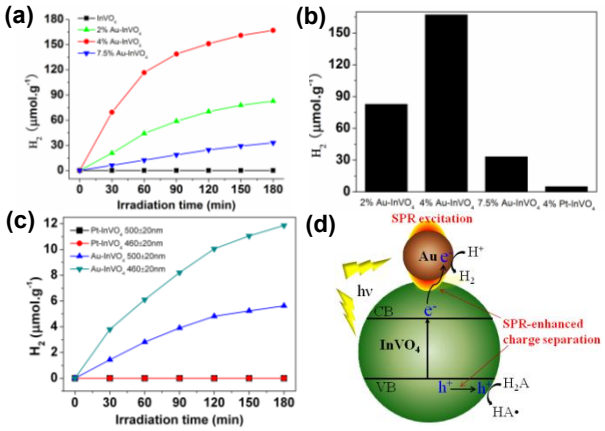

Fig. 3 (a) Plots of photocatalytic H_2 evolution amount versus irradiation ($\lambda > 420$ nm) time for different samples; (b) Comparison of H_2 evolution amount of for Au-$InVO_4$ and Pt-$InVO_4$ samples after 3h irradiation; (c) Photocatalytic H_2 evolution for 4 wt% Au-$InVO_4$ and 4 wt% Pt-$InVO_4$ under irradiation at 460±20 nm and 500±20 nm; (d) Schematic illustration of the plasmon-enhanced photocatalytic process for H_2 evolution on the Au-$InVO_4$ hybrid structure, in which H_2A and HA• refers to ascorbic acid and ascorbate radical, respectively.

To strengthen the above conclusion, we carry out further comparison tests by controlling the irradiation wavelengths at 460±20 nm and 500±20 nm, respectively. Fig. 3c indicate that in both wavelength ranges, the 4 wt% Pt-$InVO_4$ sample does not show observable H_2 evlolution, while the 4 wt% Au-$InVO_4$ sample is still quite active. This means that even though $InVO_4$ microspheres absorb photons in these two ranges through sub-band gap transition, the majority of photogenerated electrons would recombine rapidly with the holes rather than transfer to the contacted Pt nanoparticles for water reduction. Note that small Pt nanoparticles do not exhibit SPR absorption in the visible light range. So the SPR-absorption from the Au nanoparticles grown on the $InVO_4$ microspheres should play important roles in the enhanced efficiency of Au-$InVO_4$ samples.

It is known that the SPR-excitation of metal nanostructures can generate strongly enhanced localized electric fields with magnitudes up to 10^5 times of the incident energy.[29] By this way, the metal nanostructures act like optical antenna to concentrate the light energy at the near surfaces. Therefore the $InVO_4$ nanocrystals near the Au-$InVO_4$ interfaces would encounter much more intense sub-band gap excitation by this SPR-enhanced electric field, which can generate more photo-excited electrons for water reduction. Moreover, the visible-light absorption of $InVO_4$ induced by the sub-bandgap transition has been ascribed to impurities or defects in the crystal structure. But these impurities and defects can also act as recombination sites of photogenerated electrons and holes. However, the wide overlap between Au-plasmon band and $InVO_4$ absorption in the visible light range enables intensive plasmon-exciton coupling that significantly increases the exciton dissociation efficiency,[20,21] and thereby promote the photocatalytic efficiency. As a result, the photogenerated holes can oxidize L-ascorbic acid (H_2A) on the $InVO_4$ surface; meanwhile the separated electrons will have relatively longer time to reduce H^+ to H_2 on the gold nanoparticle surface. This SPR-enhanced photocatalyic process is illustrated in Fig. 3d.

It is also noted that for the Au-$InVO_4$ sample, the 460±20 nm irradiation results in higher H_2 evolution efficiency than the 500±20 nm irradiation (Fig. 3c) even though the gold nanoparticles have stronger SPR at the latter irradiation range. This means that the major contribution of the photocatalytic activity still comes from the $InVO_4$ excitation. Certainly the excitation at 460±20 nm creates more excitons than the excitation at 500±20 nm since the $InVO_4$ microspheres have stronger absorption at 460±20 nm. Even if the gold plasmon at 460 nm is relative weak, it still can provide sufficient enhancement to achieve desirable exciton dissociation yield on $InVO_4$. While under excitation at 500 nm, the stronger excitation of gold SPR at 500 nm does not show further improvement due to weaker excitation of $InVO_4$ with less available photogenerated electrons for water reduction. Nevertheless, in order to achieve good photocatalytic performance, the gold surface plasmon is still indispensable to enhance the exciton dissociation on $InVO_4$ since the Pt-$InVO_4$ sample shows no activity for H_2 evolution under the irradiation at the same wavelength range.

However, when the gold loading amount is too high, the excessive gold nanoparticles would serve as the centers to promote electron-hole recombination and thereby reduce the photocatalytic activity. That's why the 7.5 wt% Au-$InVO_4$ showed less H_2 evolution activity as comparing with the other two Au-$InVO_4$ samples. In addition, the decreased activities of the Au-$InVO_4$ samples after 90 min (Fig. 3a) are attributed to increased size of the gold nanoparticles on $InVO_4$ during the photocatalytic reaction. As shown in Fig. S9, the gold particle size changes to above 15 nm, which may be ascribed to the structure re-construction of small Au nanoparticles induced by ascorbic acid.[30] While larger gold particles have higher resistance to the etching by ascorbic acid, thus the photocatalytic activity becomes stable thereafter. Since the EDX

analysis indicates no change in the gold percentage (Fig. S9e), the conversion of gold nanoparticles from small to large size causes decrease of Au-$InVO_4$ interfaces. Therefore, the effective area of SPR enhancement is also reduced, leading to lower photocatalytic efficiency of Au-$InVO_4$ samples.

In summary, we have demonstrated the plasmon-enhanced H_2 evolution from photocatalytic water splitting by using Au-$InVO_4$ hybrid microspheres. The surface plasmons of gold nanoparticles that were grown on $InVO_4$ microspheres substantially improve the separation of photogenerated electrons and holes on $InVO_4$ through plasmon-exciton coupling. In comparison, the Pt-$InVO_4$ sample showed very little activity on H_2 evolution due to the lack of visible light SPR from Pt nanoparticles. We believe that our studies will have considerable impact on future development of more efficient plasmonic metal-semiconductor photocatalysts for visible-light-driven water splitting.

The authors acknowledge financial support from NTU Start-Up Grant (SUG), MOE AcRF-Tier1 RG 44/11, NTU seed funding for Solar Fuels Laboratory, and Singapore NRF-CRP (NRF-CRP5-2009-04) .

Notes and references

[a] *Solar Fuels Laboratory, School of Materials Science and Engineering*
Nanyang Technological University, 50 Nanyang Avenue, Singapore
639798, Singapore. E-mail: cxue@ntu.edu.sg, joachimloo@ntu.edu.sg
[b] *Division of Molecular Biosciences, Imperial College London, South Kensington Campus London SW7 2AZ, U.K.*

† Electronic Supplementary Information (ESI) available: Experimental details and additional characterization data. See DOI: 10.1039/b000000x/

1 S. Linic, P. Christopher and D. B. Ingram, *Nature. Mater.*, 2011, **10**, 911.
2 A. Iwase and A. Kudo, *J. Mater. Chem.*, 2010, **20**, 7536.
3 D. Wang, H. Jiang, X. Zong, Q. Xu, Y. Ma, G. Li and C. Li, *Chem.-Eur. J.*, 2011, **17**, 1275.
4 A. Duret and M. Grätzel, *J. Phys. Chem. B*, 2005, **109**, 17184.
5 H. Xie, Y. Z. Li, S. F. Jin, J. J. Han and X. J. Zhao, *J. Phys. Chem. C*, 2010, **114**, 9706.
6 C. H. Kuo, C. H. Chen and M. H. Huang, *Adv. Funct. Mater.*, 2007, **17**, 3773.
7 L. N. Kong, W. Chen, D. K. Ma, Y. Yang, S. S. Liu and S. M. Huang, *J. Mater. Chem.*, 2012, **22**, 719.
8 J. H. Ye, Z. G. Zou, M. Oshikiri, A. Matsushita, M. Shimoda, M. Imai and T. Shishido, *Chem. Phys. Lett.*, 2002, **356**, 221.
9 M. Oshikiri, M. Boero, J. H. Ye, Z. G. Zou and G. Kido, *J. Chem. Phys.*, 2002, **117**, 7313.
10 G. L. Li and Z. Yin, *Phys. Chem. Chem. Phys.*, 2011, **13**, 2824.
11 C. S. Enache, D. Lloyd, M. R. Damen, J. Schoonman and R. van de Krol, *J. Phys. Chem. C*, 2009, **113**, 19351.
12. K. Rakesh, S. Khaire, D. Bhange, P. Dhanasekaran, S. S. Deshpande, S. V. Awate and N. M. Gupta, *J. Mater. Sci.*, 2011, **46**, 5466.
13 H. Y. Lin, Y. F. Chen and Y. W. Chen, *Int. J. Hydrogen Energy*, 2007, **32**, 86.
14 L. X. Xu, L. X. Sang, C. F. Ma, Y. W. Lu, F. Wang, Q. W. Li, H. X. Dai, H. He and J. H. Sun, *Chin. J. Catal.*, 2006, **27**, 100.
15 Z. Liu, W. Hou, P. Pavaskar, M. Aykol and S. B. Cronin, *Nano Lett.*, 2011, **11**, 1111.
16 J.-J. Chen, J. C. S. Wu, P. C. Wu and D. P. Tsai, *J. Phys. Chem. C*, 2011, **115**, 210.
17 Z. Zheng, B. Huang, X. Qin, X. Zhang, Y. Dai and M.-H. Whangbo, *J. Mater. Chem.*, 2011, **21**, 9079.
18 M. M. Shahjamali, M. Bosman, S. W. Cao, X. Huang, S. Saadat, E. Martinsson, D. Aili, Y. Y. Tay, B. Liedberg, S. C. J. Loo, H. Zhang, F. Boey and C. Xue *Adv. Funct. Mater.* 2012, **22**, 849-854.
19 X. Huang, X. Y. Qi, Y. Z. Huang, S. Z. Li, C. Xue, C. L. Gan, F. Boey, H. Zhang, *ACS Nano* 2010, **4**, 6196-6202.
20 H. W. Gao, C. Liu, H. E. Jeong and P. Yang, *ACS Nano*, 2012, **6**, 234.
21 E. Thimsen, F. Le Formal, M. Gratzel and S. C. Warren, *Nano Lett*, 2011, **11**, 35.
22 Y. Wang, Y. H. Shen, A. J. Xie, S. K. Li, X. F. Wang and Y. Cai, *J. Phys. Chem. C*, 2010, **114**, 4297.
23 S. W. Cao, Z. Yin, J. Barber, F. Y. Boey, S. C. Loo and C. Xue, *ACS Appl. Mater. Inter.*, 2012, **4**, 418.
24 S. Link and M. A. El-Sayed, *J. Phys. Chem. B*, 1999, **103**, 4212.
25 Y. H. Wei, S. B. Han, D. A. Walker, S. C. Warren and B. A. Grzybowski, *Chem. Sci.*, 2012, DOI: 10.1039/c2sc00673a.
26 P. Li, Z. Wei, T. Wu, Q. Peng and Y. D. Li, *J. Am. Chem. Soc.*, 2011, **133**, 5660.
27 S. G. Kumar and L. G. Devi, *J. Phys. Chem. A*, 2011, **115**, 13211.
28 T. F. Jaramillo, K. P. Jørgensen, J. Bonde, J. H. Nielsen, S. Horch and I. Chorkendorff, *Science*, 2007, **317**, 100.
29 S. Y. Gao, K. Ueno and H. Misawa, *Accounts Chem. Res.*, 2011, **44**, 251.
30 C. Novo and P. Mulvaney, *Nano Lett.*, 2007, **7**, 520.